Ultraviolet photodissociation of Xe_2^+ and Kr_2^+ $1(\frac{1}{2})_u$: Detection of rare-gas dimer ions in real time

A. W. McCown, M. N. Ediger, S. M. Stazak, and J. G. Eden
Department of Electrical Engineering, University of Illinois at Urbana-Champaign, Urbana, Illinois 61801
(Received 20 December 1982)

Momentary depletion of the Xe_2^+ (or Kr_2^+) $1(\frac{1}{2})_u$ population is observed by photodissociating the molecule at 351.1, 337.1, or 307.9 nm [on the $1(\frac{1}{2})_u \rightarrow 2(\frac{1}{2})_g$ band] and monitoring the temporally resolved emission from the dissociative-recombination–fed neutral Xe line at 828.0 nm ($6p[\frac{1}{2}]_0 \rightarrow 6s[\frac{3}{2}]_1$). Near total suppression ($>90\%$) of the Xe ($6p \rightarrow 6s$) fluorescence is obtained for laser intensities of 50 MW cm^{-2}. Measurements of the absolute electron density confirm that this effect is due to depletion of the dimer-ion concentration rather than photoionization of the $6p[\frac{1}{2}]_0$ state. However, photoionization of the Xe ($6s'$ or $6p$) levels is observed and the cross section is measured to be 2.3×10^{-18} cm^2 at 351 nm. These experiments demonstrate a means for studying the collisional kinetics of rare-gas dimer ions in real time and in the presence of large background gas pressures.

An optical approach to detecting the homonuclear rare-gas ions (R_2^+) *in real time* has been demonstrated and is described in this paper. This technique involves the bound-to-free $[1(\frac{1}{2})_u \rightarrow 2(\frac{1}{2})_g]$ ultraviolet absorption band of the diatomic rare-gas ions which for several years has been recognized as having an adverse effect on the performance of high-pressure ($\gtrsim$ 1bar) lasers employing a rare-gas buffer.[1,2] Specifically, it has been shown that an ultraviolet laser (XeF, 351.1 nm; N_2, 337.1 nm; or XeCl, 307.9 nm) can be used to photodissociate Xe_2^+ or Kr_2^+ $1(\frac{1}{2})_u$ ions and that the momentary depletion of the molecular-ion population is detectable by observing the temporally resolved electron density and the spontaneous emission due to transitions between two excited states of the neutral rare-gas atom.

Consequently, the Xe_2^+ $1(\frac{1}{2})_u$ species can be selectively (and rapidly) removed from the kinetic formation chain of another molecular or atomic species of interest. Therefore, the extent of the ion's participation in diverse chemical processes can be identified while monitoring the R_2^+ population in real time. Of the few techniques that are available for the detection of molecular ions, most (such as mass spectroscopy) lack this ability, which hinders the study of the collisional kinetics of the ion.

Viewed another way, the recombination of R_2^+ ions can now be prevented without heating the plasma electrons. Goldstein, Anderson, and Clark[3] demonstrated that the strong electron temperature dependence of the R_2^+ dissociative-recombination rate constant can be exploited to slow the loss of molecular ions to recombination. Since then, pulsed microwave[4] (or discharge)[5] heating of the electrons in low-pressure, weakly ionized plasmas has proven to be a useful tool for studying the neutral products of dissociative recombination in all of the rare gases.[4–6]

Figure 1 shows the relevant energy levels of Xe and Xe_2. Nonresonant photoionization of Xe at 193 nm using an ArF laser produces an Xe^+ ($^2P_{3/2}$ core) ion and a 0.7-eV electron.[7] Theoretical and experimental values for the two-photon cross section for this process have recently been reported.[7–10] For Xe pressures above 100 Torr, the atomic ions rapidly ($\tau < 1$ μs) dimerize by the three-body collisional process:

$$Xe^+(^2P_{3/2}) + 2Xe(^1S_0) \xrightarrow{k_f} Xe_2^+[1(\tfrac{1}{2})_u] + Xe(^1S_0)\ , \quad (1)$$

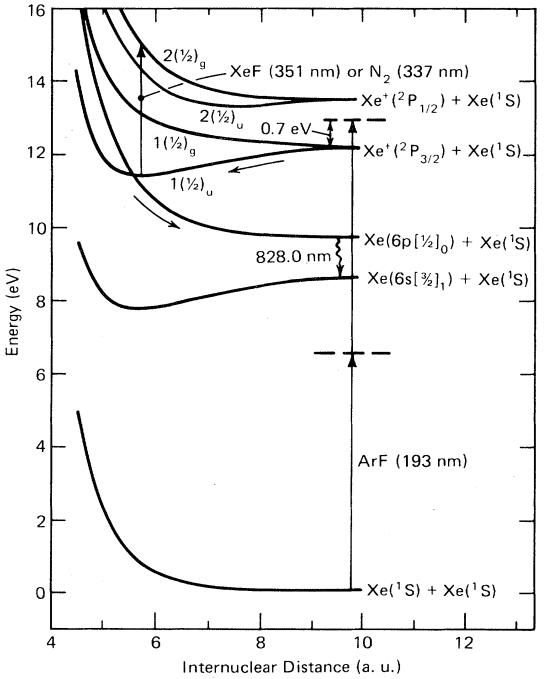

FIG. 1. Partial energy-level diagram of atomic and molecular xenon showing two photon ionization of Xe at 193 nm ($\hbar\omega = 6.4$ eV) followed by photodissociation of Xe_2^+ $1(\frac{1}{2})_u$ at 351 nm ($\hbar\omega = 3.5$ eV). Adapted from Refs. 12 and 26.

yielding Xe_2^+ in its ground state.

Normally, the predominant loss channel for Xe_2^+ ions is dissociative recombination with cool electrons:

$$Xe_2^+[1(\tfrac{1}{2})_u]+e^- \underset{\alpha}{\rightarrow} Xe^*+Xe(^1S_0)\,, \tag{2}$$

where the asterisk denotes an electronically excited state of the neutral atom and α is the recombination coefficient expressed in $cm^3\,sec^{-1}$ and is a function of the electron temperature T_e. The xenon $6p$ levels are strongly fed in this process and subsequently radiate in the near infrared.[6]

The subsequent arrival of a second uv laser pulse ($250 \leq \lambda \leq 350$ nm) depletes the Xe_2^+ population by photodissociating the molecule via the $1(\frac{1}{2})_u \rightarrow 2(\frac{1}{2})_g$ band. Thus, the dissociative-recombination term that feeds the $Xe^*(6p)$ manifold of states collapses. Owing to the ~30-ns radiative lifetime of the Xe $6p[\frac{1}{2}]_0$ level and the rapid quenching of the state by neutral xenon atoms,[11] the Xe* spontaneous emission decays rapidly and the degree of fluorescence suppression is dependent upon the percentage of the Xe_2^+ population that is dissociated. The strong quenching of Xe* atoms by the background Xe also insures that the temporal behavior of the $6p \rightarrow 6s$ fluorescence nearly mirrors that of the Xe_2^+ population. Therefore, in the experiments to follow, the temporal history of the $Xe_2^+\,1(\frac{1}{2})_u$ population is monitored indirectly by observing the Xe $6p[\frac{1}{2}]_0 \rightarrow 6s[\frac{3}{2}]_1$ emission line at 828.0 nm, although the lines at 823.2 and 881.9 nm could serve the same purpose.

The R_2^+ ultraviolet absorption continua have been extensively studied from a theoretical standpoint and a detailed summary of their optical properties can be found in Ref. 12. For Xe_2^+, the peak $1(\frac{1}{2})_u \rightarrow 2(\frac{1}{2})_g$ absorption cross section of $\sim 3.6\times 10^{-17}$ cm^2 (300 K) occurs near 340 nm and the full width at half maximum (FWHM) of the band is ~85 nm. As shown in Fig. 1, the $Xe_2^+\,2(\frac{1}{2})_g$ state is dissociative and its asymptotic limit is $Xe^+(^2P_{1/2})+Xe$. Experimental measurements of the R_2^+ ultraviolet photodissociation cross sections by drift tube mass spectroscopy have been reported[13] previously, but were relegated to wavelengths above 350 nm whereas the theory predicts maximum absorption for $\lambda \lesssim 340$ nm. The approach described here also permits the determination (in pulsed, low repetition rate experiments) of $1(\frac{1}{2})_u \rightarrow 2(\frac{1}{2})_g$ absorption to the blue (short-wavelength) side of the theoretical maximum.

The experimental apparatus consists primarily of two excimer lasers [one operating on the ArF band at 193 nm and the other on XeF(351.1 nm), XeCl(307.9 nm), or N_2(337.1 nm)] whose rectangular [$\sim 2.9 \times (0.7-1.0)$cm^2] beams are focused into a quartz cell (to an area of 0.02×2.9 cm^2) and the relative timing between the two laser pulses is adjusted by means of a digital delay generator. A separate quartz cell was made for each Xe pressure studied and details regarding outgassing and filling of the rare-gas cells and the optical characteristics of the excimer laser beams have been described previously.[7,11]

Temporally resolved measurements of the absolute electron density were performed[7] by placing the Xe cells in a section of cylindrical X-band waveguide and recording the single pass attenuation of a 9.252-GHz probe signal during and following the firing of each excimer laser. Rectangular slots machined into the side walls of the cylindrical waveguide permit the entry of the laser beams. Also, a 6-mm-diam hole drilled into a waveguide elbow allows for monitoring the Xe 828.0-, 823.2- ($6p[\frac{3}{2}]_2 \rightarrow 6s[\frac{3}{2}]_2$), and 881.9-nm ($6p[\frac{5}{2}]_3 \rightarrow 6s[\frac{3}{2}]_2$) transitions with an RCA C31034A photomultiplier (GaAs photocathode) and one of several dielectric bandpass filters ($\Delta\lambda_{FWHM} \sim 10$ nm). Spectral surveys of the Xe emission were conducted with a 0.6-m spectrograph (in first order) and an optical multichannel analyzer.

A series of photographs illustrating the depletion of the $Xe_2^+\,1(\frac{1}{2})_u$ population by photodissociation at 351 nm is shown in Fig. 2. Xe* ($6p[\frac{1}{2}]_0 \rightarrow 6s[\frac{3}{2}]_1$) fluorescence waveforms (heavy solid curves) are given for various time delays ($50 \leq \Delta t \leq 250$ ns) between the ArF and XeF laser pulses. The photos depict an upward increase in intensity and the arrival of the XeF pulse at the Xe cell is evidenced by the sudden decline in the Xe* fluorescence intensity. For these data, the Xe pressure is 300 Torr and I_{ArF} and I_{XeF} are 125 and 50 MW cm^{-2}, respectively. The curves in Fig. 2(a) indicate the shape of the Xe* fluorescence waveform in the absence of a dissociating laser pulse.

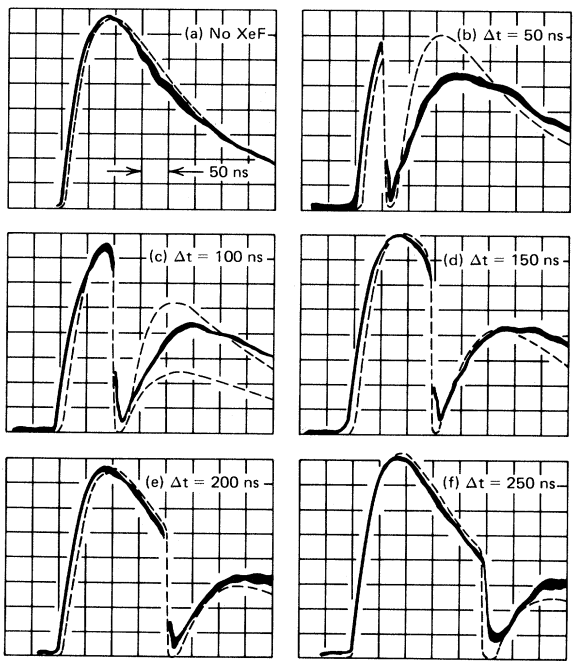

FIG. 2. Oscillograms of Xe* ($6p[\frac{1}{2}]_0 \rightarrow 6s[\frac{3}{2}]_1$) fluorescence at 828.0 nm illustrating suppression of the $Xe_2^+\,1(\frac{1}{2})_u$ population for various time delays (Δt) between the ArF and XeF lasers. The dashed profiles in (a)—(f) represent the predictions of the computer code discussed in the text. In (a), the profile of the unperturbed Xe* waveform is indicated by both curves. For these data, the ArF and XeF laser intensities are 125 and 50 MW cm^{-2}, respectively, and $p_{Xe}=300$ Torr.

Clearly, the onset of suppression closely follows XeF irradiation of the gas and depressions greater than 90% are routinely observed. Maximum quenching of the Xe* fluorescence is, of course, dependent on the degree of spatial overlap of the two uv laser beams. Similar behavior was observed for the Xe 823.2- and 881.9-nm lines and for $p_{Xe}=100$ Torr.

The predictions of a computer kinetics model are also shown (dashed curves) in Fig. 2. Differential equations describing the temporal production and destruction of the $Xe^+(^2P_{3/2})$, $Xe_2^+\,1(\frac{1}{2})_u$, and $Xe\,6p[\frac{1}{2}]_0$ species were numerically integrated with an Adams-Moulton algorithm. Two-photon ionization of Xe at 193 nm is assumed to be the sole production term for the $^2P_{3/2}$ ion and the pumping rate is

$$\beta(I_{ArF})^2[Xe](\hbar\omega_{ArF})^{-1}\,,$$

where

$$\beta=(4\pm1)\times10^{-32}\text{cm}^4\,\text{W}^{-1}$$

(Refs. 7 and 14). Molecular xenon ions are formed in the $1(\frac{1}{2})_u$ state by reaction (1) (where k_f was taken to be 1.0×10^{-31} $\text{cm}^6\,\text{s}^{-1}$) (Ref. 15) and collisionally lost through dissociative recombination with 0.7-eV electrons[16] ($\alpha=2.5\times10^{-7}$ $\text{cm}^3\,\text{s}^{-1}$).[6] Photodissociation of Xe_2^+ on the $1(\frac{1}{2})_u\rightarrow2(\frac{1}{2})_g$ band at 351 nm is governed by a cross section of $\sim3.4\times10^{-17}$ cm^2 (Ref. 12) and radiative and collisional deactivation of the $Xe\,6p[\frac{1}{2}]_0$ state have also been incorporated into the model ($\tau_{sp}=29$ ns, $k_Q=4\times10^{-10}$ $\text{cm}^3\,\text{s}^{-1}$).[11]

The products of the photodissociation of $Xe_2^+\,1(\frac{1}{2})_u$ at 351 nm are an $Xe^+(^2P_{1/2})$ ion and a ground-state Xe atom. Although the $Xe^+(^2P_{1/2}\rightarrow{}^2P_{3/2})$ transition is electric dipole forbidden[17] and the collisional-radiative charge transfer process

$$Xe^+(^2P_{1/2})+Xe(^1S_0)\rightarrow Xe^+(^2P_{3/2})+Xe(^1S_0)+\hbar\omega(1.3\text{ eV}) \quad (3)$$

is expected to be slow, Helm and Varney[18] have shown that $Xe^+(^2P_{1/2})$ rapidly forms the $Xe_2^+\,2(\frac{1}{2})_u$ ion in a three-body process similar to (1). Subsequent radiative decay on the $2(\frac{1}{2})_u\rightarrow1(\frac{1}{2})_g$ (bound→free) band of Xe_2^+ replenishes the $Xe^+(^2P_{3/2})$ population. Thus, $Xe_2^+\,1(\frac{1}{2})_u$ molecules are eventually reformed and the recovery time, which depends on the sum of 2 three-body collisional formation rates, is 100–200 ns ($p_{Xe}=300$ Torr) for rate constants on the order of 10^{-31} $\text{cm}^6\,\text{s}^{-1}$.

To simplify the model, an arbitrary fraction δ of the photodissociated $Xe_2^+\,1(\frac{1}{2})_u$ molecules is assumed to immediately result in $Xe^+(^2P_{3/2})$ ions. Figure 2(c) shows the theoretical profiles obtained when δ is 1.0 (upper dashed curve) or 0 (i.e., all dissociated molecules are permanently removed from the kinetic chain). Fluorescence recovery occurs in the latter case since the Xe^+ population continues to feed the $Xe_2^+\,1(\frac{1}{2})_u$ species although the atomic ion concentration is only a fraction of its peak value. Each of the other model curves (b, d, e, and f) assume that $\delta=1.0$. Details of the kinetics model will be described elsewhere.

The recovery time of the spontaneous emission waveforms in Fig. 2 (100–150 ns) is consistent with a sudden depletion of the population of the Xe* precursor (Xe_2^+). A much more rapid recovery time (<10 ns) is required if photoionization of the $Xe\,6p[\frac{1}{2}]_0$ state is presumed to be responsible for the 828.0-nm fluorescence suppression. Also note that, following the second laser pulse, the experimental waveforms generally resume their normal decay more slowly than do the theoretical curves. This is possibly due to the $Xe^+(^2P_{1/2}\rightarrow{}^2P_{3/2})$ collisional deactivation sequence mentioned earlier.

Results similar to those in Fig. 2 were obtained when an N_2 laser ($\lambda=337$ nm) supplied the second optical pulse except that smaller fluorescence suppressions were observed due to the lower laser energies available. Suppressions equivalent in magnitude to those at 351 nm were recorded when an XeCl laser (308 nm) was employed. However, this effect was not observed for $\lambda=248$ nm (KrF) even though intensities ~3 times larger than those at 351 nm were used. Thus, the absorption process responsible for quenching the Xe_2^+ recombination emission is indeed broadband and the continuum's bandwidth is consistent with Wadt's theory. Comparable results were obtained for Kr_2^+ when the Kr atom was ionized by three ArF photons and recombination emission was monitored via the $5p[\frac{1}{2}]_0\rightarrow5s[\frac{3}{2}]_1$ line at 758.7 nm.

Representative results of microwave measurements of the temporal history of the photoelectron density in 300-Torr Xe($I_{ArF}=100$ $\text{MW}\,\text{cm}^{-2}$) are presented in Fig. 3. The heavy curve is the microwave absorption signal as observed on the oscilloscope while the dashed waveform is the experimental trace after correcting for the saturation of the detection system above $n_e\simeq2\times10^{13}$ cm^{-3} (cf. Ref. 7). The prediction of the kinetics model is denoted by the thin solid curve.

If one varies the time delay (Δt) between the ArF pump and XeF dissociating laser pulses, the waveforms illustrat-

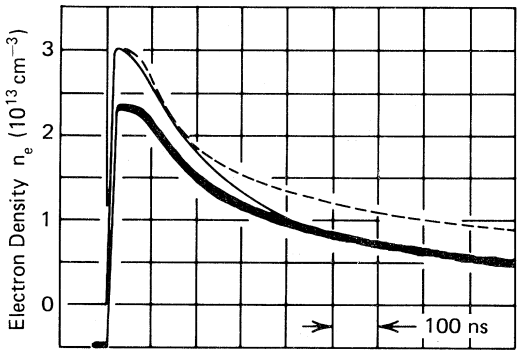

FIG. 3. Typical microwave absorption waveform (heavy curve) and absolute electron density (dashed curve) which has been corrected for saturation of the microwave detection system (i.e., departure from I_{ArF}^2 dependence for $n_e\gtrsim2\times10^{13}$ cm^{-3}). Also shown is the model prediction (thin solid profile). The ArF laser intensity is 100 $\text{MW}\,\text{cm}^{-2}$ and $p_{Xe}=300$ Torr.

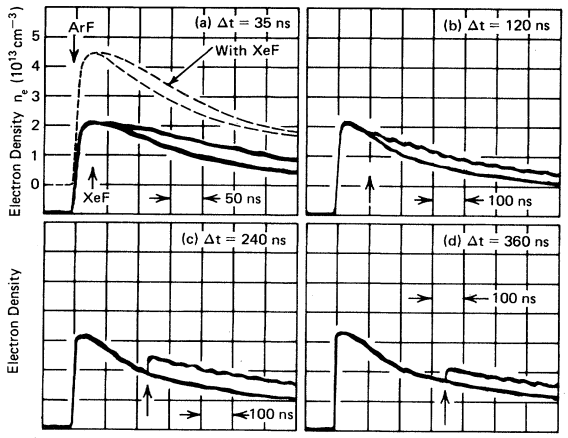

FIG. 4. Absolute electron-density waveforms for various time delays between the ArF and XeF laser pulses. Also shown in (a) are the theoretical electron-density waveforms in the presence and absence of the XeF laser pulse ($\Delta t = 35$ ns). For all of these traces, $I_{ArF} = 130$ MW cm^{-2}, $I_{XeF} = 30$ MW cm^{-2} and $p_{Xe} = 300$ Torr.

ed in Fig. 4 are observed. The results for several values of Δt are shown. For $\Delta t \lesssim 120$ ns, firing the XeF laser ($I_{XeF} \sim 30$ MW cm^{-2}) briefly interrupts the decay of the electron density which is exactly what would be expected if the Xe_2^+ population were temporarily depleted. Secondly, the electron density curves ($\Delta t = 35$ and 120 ns) return to the slope of the "unperturbed" waveform ~ 100 ns after the XeF pulse is terminated. This behavior is again consistent with the Xe_2^+ collisional formation time constant ($(k_f[Xe]^2)^{-1} \simeq 115$ ns at 300 Torr) and indicates that the Xe_2^+ population (and dissociative-recombination rate) has, by this time, fully recovered. The theoretical curves shown in Fig. 4(a) confirm that this is the expected behavior for n_e. Finally, since for $\Delta t \leq 120$ ns there is no

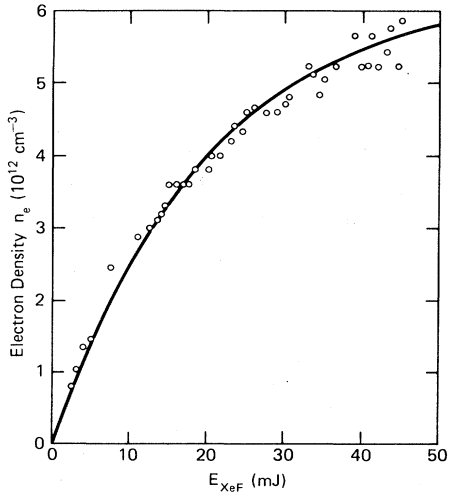

FIG. 5. Dependence of the excess electron density Δn_e on the XeF laser pulse energy. The best fit of Eq. (6) to the data yields a photoionization cross section of 2.3×10^{-18} cm^2. The ArF laser intensity is 112 MW cm^{-2} and Δt is fixed at 250 ns.

increase in n_e when the XeF pulse arrives (even though the Xe* population is near its peak value—cf. Fig. 2), the suppression of the Xe* 828-nm fluorescence in Fig. 2 is not due to photoionization of the $6p[\frac{1}{2}]_0$ state at 351 nm but rather to the loss of Xe_2^+ ions by photodissociation.

For longer time delays between the ArF and XeF lasers ($\Delta t = 240$ and 360 ns), the electron density is experimentally observed to abruptly increase by as much as $(5-8) \times 10^{12}$ cm^{-3} and the "unperturbed" and "perturbed" waveforms follow each other from that point on. This increase in the electron density,[19] Δn_e, arises due to photoionization of an excited state lying lower in energy than the Xe $6p[\frac{1}{2}]_0$ level. To determine the photoionization cross section (at 351 nm) and identity of this state, the coupled rate equations

$$\frac{dN^*}{dt} = -\frac{\sigma_{PI} I_{XeF}}{\hbar\omega} N^* = -\frac{d(\Delta n_e)}{dt} \tag{4}$$

were solved where N^* is the population density and σ_{PI} is the photoionization cross section for the excited state in question. Following the termination of the XeF laser pulse, the solutions to (4) are

$$N^* = N_0 \exp\left[-\frac{\sigma_{PI} E_{XeF}}{\hbar\omega A}\right] \tag{5}$$

and

$$\Delta n_e = N_0 \left[1 - \exp\left[-\frac{\sigma_{PI} E_{XeF}}{\hbar\omega A}\right]\right], \tag{6}$$

where N_0 is the excited-state population immediately prior

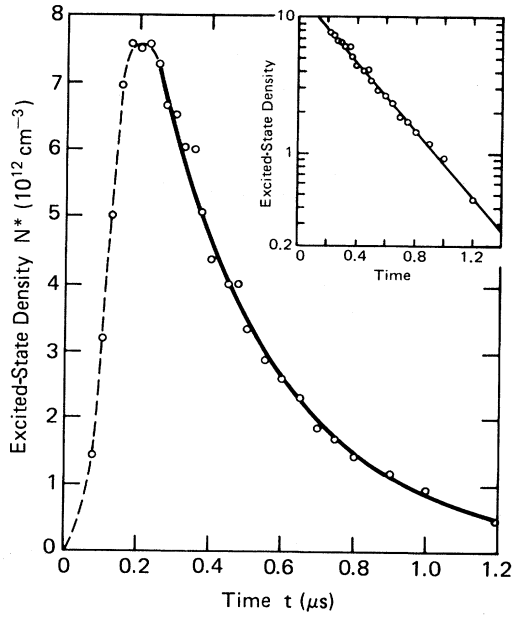

FIG. 6. Temporal history of the excited-state density N^*. Solid line drawn through the data points is an exponential with a decay constant of 2.9×10^6 s^{-1}. A semilog plot of the same data is shown in the inset (vertical axis—same units). Xe pressure is 300 Torr, I_{ArF} is again 112 MW cm^{-2}, and the ArF laser is fixed at $t = 0$.

to the arrival of the XeF pulse and A is the beam area as it traverses the Xe cell. Also, the excited-state production term is assumed to be negligible during the XeF pulse. Equations (4) were integrated assuming a triangular XeF laser pulse with rise (zero-to-peak) and fall times of 8 and 17.6 ns, respectively.

Figure 5 illustrates the variation of Δn_e as E_{XeF} is adjusted between 2.5 and 45 mJ/pulse where the XeF laser is delayed with respect to the ArF pump by 250 ns. The solid line drawn through the data obeys the relationship

$$\Delta n_e = 6.3\times 10^{12}[1-\exp(-0.0504E_{\mathrm{XeF}})]\ , \tag{7}$$

where E_{XeF} is expressed in mJ and Δn_e in cm^{-3}. From (7) σ_{PI} is determined to be $(2.3\pm 0.5)\times 10^{-18}$ cm^2.

As the XeF pulse energy becomes large, the excess electron density saturates—that is, $\Delta n_e \rightarrow N_0$. Therefore, the temporal behavior of N^* was determined by measuring the saturated excess electron density (from the Δn_e vs E_{XeF} profile) for various time delays between the ArF and XeF lasers.

The variation of N^* following the ArF pump pulse is shown in Fig. 6. In contrast to the Xe $6p[\frac{1}{2}]_0$ population which peaks at $t\sim 100$ ns, N^* reaches its maximum value ~ 200 ns after the ArF laser is fired. Also, the temporal decay of the N^* species concentration is best described by a single exponential (as shown by the solid line in Fig. 6) having a decay constant of 2.9×10^6 s^{-1}. If the loss of atoms (N^*) in the excited-state is attributed solely to the formation of Xe_2^* by three-body collisions, then this decay rate corresponds to a molecular production rate constant of 3×10^{-32} $\mathrm{cm}^6\mathrm{s}^{-1}$, which is consistent with values in the literature for the deexcitation of the $^3P_2$ and $^3P_0$ members of the Xe($6s$) manifold.[20,21]

These results suggest that a low-lying metastable state of neutral Xe is being photoionized. The energy of an XeF photon (351 nm:28 482 cm^{-1}) requires that an Xe* energy level above $\sim 69\,300$ cm^{-1} be involved which implicates either the $6s'[\frac{1}{2}]_0$ state or energy levels in the $6p$ manifold. However, since radiation trapping is important at these high pressures, it is impossible at this point to exclude resonant states such as $6s'[\frac{1}{2}]_1$. The photoionization cross section determined earlier can also be estimated by setting $\sigma_{PI} I_{\mathrm{XeF}}(\hbar\omega_{\mathrm{XeF}})^{-1}$ equal to the excess electron production rate ($\sim 10^{20}$ $\mathrm{cm}^{-3}\mathrm{s}^{-1}$). The result, $\sigma_{PI}\approx 2\times 10^{-18}$ cm^2, is close to the experimentally determined value and both are somewhat smaller than cross sections calculated by Chang[22] for photoionization of the p states of Xe. In contrast, they are an order of magnitude larger than excited s-state ionization cross sections for Ar and Kr.[23]

Little data can be found in the literature regarding photoionization of the rare-gas s' states. Stebbings *et al.*[24] have demonstrated an enhancement in the photoionization of s and s' levels in Ar, Kr, and Xe due to autoionization but were unable to measure absolute cross sections. Several $6s'[\frac{1}{2}]_0 \rightarrow np'[\frac{1}{2}$ or $\frac{3}{2}]_1$ autoionizing transitions between 441 and 376 nm were observed, raising the possibility that such a transition is involved here. When the wavelength of the second laser pulse is 248 nm (KrF) rather than 351 nm, no immediate increase in electron density is observed, which places an upper limit of $\sim 8\times 10^{-20}$ cm^2 on the photoionization cross section at this wavelength.

From the experimental evidence presented here, it is concluded that Xe_2^+ or Kr_2^+ ions can be photodissociated with an ultraviolet laser pulse and that the sudden depletion of the ground-state ion concentration is detectable from the temporally resolved electron density and by observing the spontaneous emission occurring between two neutral atomic states. Also, microwave diagnostics permit the measurement of neutral excited-state photoionization cross sections—a technique that would be improved with the use of a narrow linewidth dye laser rather than the broadband excimer laser employed here. The applications of this effect to studying the participation of Xe_2^+ or Kr_2^+ in various chemical reactions, such as the formation of the XeO and Kr_2F excimer molecules, appear to be extensive.

It is interesting to note that Kaplafka *et al.*[25] observed a similar effect in 1969 when they demonstrated that the afterglow of a helium discharge could be partially quenched by irradiating the plasma with a CO_2 laser ($0.11\leq\hbar\omega\leq 0.14$ eV). While not able to pinpoint the mechanism responsible for quenching the visible afterglow radiation, they suggested that it "... appears to originate from photon-induced change of population of a state or states of a neutral or ionic helium molecule.[25]"

The authors wish to thank J. T. Verdeyen for several interesting discussions and the excellent technical assistance of K. Kuehl and Y. Moroz is appreciated. Also, the support of this work by the National Science Foundation (through R. E. Rostenbach) under grants CPE-80-06378 and CPE-80-26508 is gratefully acknowledged.

[1]See C. A. Brau, in *Excimer Lasers,* edited by C. K. Rhodes (Springer, Berlin, 1979), pp. 94—96.

[2]R. S. F. Chang and L. F. Champagne, Appl. Phys. Lett. 36, 879 (1980); L. F. Champagne, *ibid.* 35, 516 (1979).

[3]L. Goldstein, J. M. Anderson, and G. L. Clark, Phys. Rev. 90, 486 (1953).

[4]J. N. Bardsley and M. A. Biondi in *Advances in Atomic and Molecular Physics,* edited by D. R. Bates (Academic, New York, 1970), Vol. 6, pp. 16—19 and references cited therein.

[5]A. W. Johnson and J. B. Gerardo, Phys. Rev. A 5, 1410 (1972).

[6]Y-J. Shiu, M. A. Biondi, and D. P. Sipler, Phys. Rev. A 15, 494 (1977).

[7]A. W. McCown, M. N. Ediger, and J. G. Eden, Phys. Rev. A 26, 3318 (1982).

[8]W. K. Bischel, J. Bokor, D. J. Kligler, and C. K. Rhodes, IEEE J. Quantum Electron. QE-15, 380 (1979).

[9]R. V. Hodges, L. C. Lee, and J. T. Moseley, Int. J. Mass Spectrom. Ion Phys. 39, 133 (1981).

[10]E. J. McGuire, Phys. Rev. A 24, 835 (1981).
[11]A. W. McCown, M. N. Ediger, and J. G. Eden, Phys. Rev. A 26, 2281 (1982).
[12]W. R. Wadt, J. Chem. Phys. 68, 402 (1978); 73, 3915 (1980).
[13]See J. A. Vanderhoff, J. Chem. Phys. 68, 3311 (1978); L. C. Lee and G. P. Smith, Phys. Rev. A 19, 2329 (1979) and references cited therein.
[14]The two-photon ionization cross section is normally denoted as α but β is used here to avoid confusion with the dissociative-recombination rate constant.
[15]A. K. Bhattacharya, Appl. Phys. Lett. 17, 521 (1970).
[16]The electron thermalization time for $p_{Xe}=300$ Torr $\{[2m/M)\nu_m]^{-1}\rightarrow 3\ \mu s\}$ is considerably longer than the time scale of these experiments and so the initial electron temperature is adopted here. See Ref. 7.
[17]P. B. Armentrout, D. W. Berman, and J. L. Beauchamp, Chem. Phys. Lett. 53, 255 (1978).
[18]H. Helm and R. N. Varney, J. Chem. Phys. 68, 5301 (1978).
[19]As the model is normally structured, the theoretical curves for $\Delta t=240$ and 360 ns (not shown) also plateau following the XeF laser pulse since Xe^* states lower than $Xe\,6p[\frac{1}{2}]_0$ were not included in the model. Incorporating photoionization of low-lying Xe excited states into the model does allow for the sudden increase in n_e to be reproduced.
[20]J. K. Rice and A. W. Johnson, J. Chem. Phys. 63, 5235 (1975).
[21]R. Boucique and P. Mortier, J. Phys. D 3, 1905 (1970).
[22]T. N. Chang and Y. S. Kim, Phys. Rev. A 26, 2728 (1982).
[23]K. J. McCann and M. R. Flannery, Appl. Phys. Lett. 31, 599 (1977); M. R. Flannery, Ann. Phys. 79, 480 (1973).
[24]R. F. Stebbings, F. B. Dunning, and R. D. Rundel, in *Atomic Physics 4*, edited by G. Zu Putlitz, E. W. Weber, and A. Winnacker (Plenum, New York, 1975), pp. 713—730.
[25]J. P. Kaplafka, H. Merkelo, and L. Goldstein, Appl. Phys. Lett. 15, 113 (1969).
[26]E. W. McDaniel, M. R. Flannery, E. W. Thomas, H. W. Ellis, K. J. McCann, S. T. Manson, J. W. Gallagher, J. R. Rumble, E. C. Beaty, and T. G. Roberts, Compilation of Data Relevant to Nuclear Pumped Lasers, Vol. 3, Technical Report H-78-1, U.S. Army Missile Research and Development Command, Redstone Arsenal, Alabama, December, 1978 (unpublished).